CHEMISTRY
A EUROPEAN JOURNAL

DOI: 10.1002/chem.200801144

Three-Dimensional Encapsulation of Live Cells by Using a Hybrid Matrix of Nanoparticles in a Supramolecular Hydrogel

Masato Ikeda,[a] Shiori Ueno,[a] Shinji Matsumoto,[a] Yusuke Shimizu,[a] Harunobu Komatsu,[a] Ken-ichi Kusumoto,[b] and Itaru Hamachi*[a]

Abstract: From a library of glyco-lipid mimics with muconic amide as the spacer, we found that **1**, a glyco-lipid that has *N*-acetyl glucosamine and methyl cyclohexyl groups as its hydrophilic head and hydrophobic tails, respectively, formed a stable hydrogel (0.05 wt %) through hierarchical self-assembly of the lipid molecules into supramolecular nanofibers. The formation of the supramolecular hydrogel was verified by rheological measurements, and the supramolecular nanofiber was characterized as the structural element by transmission electron microscopy and atomic force microscopy observations. Absorption and circular dichroism spectroscopic measurements revealed that the muconic amide moieties of **1** are arranged in a helical, stacked fashion in the self-assembled nanofibers. Moreover, we unexpectedly found that the homogeneous distribution of the supramolecular nanofibers of **1** was greatly facilitated by the addition of polystyrene nanobeads (100–500 nm in diameter), as evaluated by confocal laser scanning microscopic observations. It is interesting that the obtained supramolecular hybrid matrix can efficiently encapsulate and distribute live Jurkat cells in three dimensions under physiological conditions. This supramolecular hybrid matrix is intriguing as a unique biomaterial.

Keywords: cell encapsulation · hydrogels · nanobeads · self-assembly · supramolecular chemistry

Introduction

Supramolecular hydrogels[1,2] composed of low-molecular-weight hydrogelators have recently received increased attention as unique matrices for cell culture and encapsulation because of their intriguing features, such as a unique formation process based on self-assembly, a flexible molecular design, rich chemical functionality, and well-defined nanostructures, which are distinct from conventional polymer gels.[3–6] In their pioneering work, S. Zhang et al. reported that a designed peptide that forms a hydrogel through β-sheet structures can be employed as a 3D cell-culture matrix for the encapsulation of a variety of mammalian cell lines.[3] S. I. Stupp et al. designed and synthesized derivatives of an amphiphilic pentapeptide epitope (IKVAV; Ile-Lys-Val-Ala-Val) found in neurite-promoting laminin, and found that the resultant hydrogel could encapsulate neural progenitor cells and induce selective differentiation of the cell into neurons owing to the high epitope density on the surface of the supramolecular nanofibers.[4] Subsequently, D. J. Pochan, J. P. Schneider et al. demonstrated that a peptide-type supramolecular hydrogel that contained stem cells could be delivered to a target site by using the mechanical responsiveness, that is, the so-called thixotropy, of the hydrogel.[5]

In contrast with these peptide-based supramolecular hydrogels, which show great promise for tissue engineering and various cell culture/assay systems, the potential utility of saccharide-based supramolecular hydrogels has not been explored yet. Saccharide and its glyco-conjugates are naturally abundant in extracellular matrices in the form of glycoproteins and as proteoglycans (heparin sulfate, chondroitin sulfate, hyaruronic acid, etc) that are similar to peptides/proteins.[7] It is also known that the saccharides displayed on a cell's surface play important biological roles in intercellular

[a] Dr. M. Ikeda, S. Ueno, Dr. S. Matsumoto, Y. Shimizu, H. Komatsu, Prof. I. Hamachi
Department of Synthetic Chemistry and Biological Chemistry
Graduate School of Engineering, Kyoto University
Katsura, Kyoto, 615-8510 (Japan)
Fax: (+81)75-383-2759
E-mail: ihamachi@sbchem.kyoto-u.ac.jp

[b] Dr. K.-i. Kusumoto
Biotechnology and Food Research Institute
Fukuoka Industrial Technology Center, 1465-5 Aikawa Kurume
Fukuoka 839–0861 (Japan)

Supporting information for this article is available on the WWW under http://dx.doi.org/10.1002/chem.200801144.

communication and cell differentiation.[8] Therefore, saccharide-based hydrogels could become a unique matrix for the immobilization and encapsulation of live cells. We first reported that several glyco-lipid mimics with sugars in the hydrophilic head and two alkyl chains in the hydrophobic tail were able to form transparent hydrogels.[9,10] From the basis of this scaffold, hydrogels that are more stable and sufficiently strong for cell culture study are being explored. Herein, we describe glyco-lipid **1**, which has muconic amide as the spacer and GlcNAc (*N*-actetyl glucosamine) as the head and which can form a stable hydrogel. More importantly, when the hierarchical self-assembly of the lipid molecules into supramolecular nanofibers was examined by various spectroscopic and microscopy measurements, we unexpectedly found that the homogeneous 3D dispersion of the supramolecular nanofibers networks was greatly facilitated by the addition of polystyrene nanobeads. It is significant that the resultant hybrid supramolecular matrix can encapsulate live Jurkat cells in three dimensions under physiological conditions.

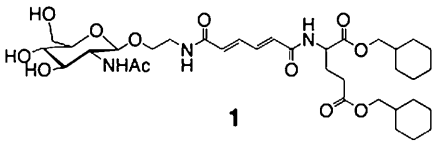

1

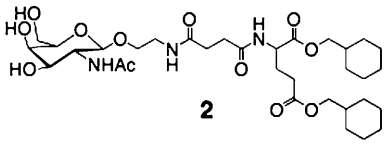

2

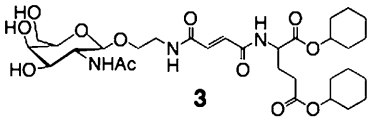

3

Results and Discussion

Synthesis and screening of the hydrogelator with muconic amide as spacer: Working from our molecular scaffolds of glyco-lipid mimicking supramolecular hydrogelators, compounds **2** and **3** with succinic and fumaric amide, respectively, as the spacer,[9,10] we replaced the spacer unit with muconic amide and constructed a new library to explore more stable hydrogels. Recently, we found that the critical gel concentration (CGC) of **3** with a fumaric amide spacer is lower than that of hydrogelators with a succinic amide spacer, such as **2**.[10] It was assumed that the rigidity and the cohesion propensity of the fumaric amide moiety could enhance the self-assembling character to form a hydrogel. This finding prompted us to increase the number of double bonds from one (fumaric) to two (muconic), and to vary the head and tail modules. The hydrogel formation ability of ten new compounds was examined by a conventional vial-inversion method.[1] Figure 1a summarizes the CGC results for

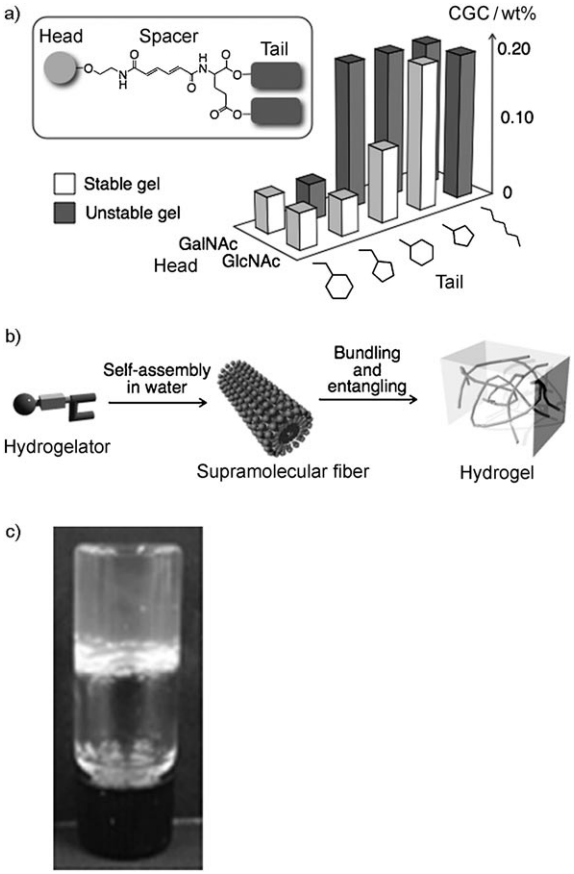

Figure 1. a) CGC values for a small combinatorial library of muconic amide hydrogelators, b) a schematic representation of the hierarchical self-assembly of hydrogelator **1**, and c) a photograph of hydrogel **1** (0.10 wt%, distilled water).

each of the new hydrogels. Apparently, the library based on the muconic amide spacer provided a larger number of hydrogelators compared with those with succinic amide and fumaric amide.[9,10] From this library, we found that glyco-lipid hydrogelator **1**, with GlcNAc as the head and methyl cyclohexyl groups as the tail, is an excellent hydrogelator (CGC = 0.05 wt%). The CGC of hydrogelator **1** is four-fold lower than that of **2** (CGC = 0.1 wt%)[9a] and is comparable to that of **3** (CGC = 0.05 wt%).[10a]

Characterization of the supramolecular hydrogel of a glyco-lipid with muconic amide as the spacer: We further characterized supramolecular hydrogel **1** in detail. Frequency-sweep rheometry measurements were conducted first. As shown in Figure 2a, the storage modulus (G'; 180 Pa at 0.9 rad s^{-1}) of hydrogel **1** (0.15 wt%, distilled water) was around six times higher than the loss modulus (G''), and both modules were almost independent of frequency, which clearly verifies the viscoelastic feature of hydrogel **1**. Transmission electron microscopy (TEM) observations of hydrogel **1** (Figure 2b) showed a well-defined network of nanofibers that have a high aspect ratio, that is, several tens of nm in diameter and hundreds of nm to a few μm in length. These are characteristics of a supramolecular gel[1] and indi-

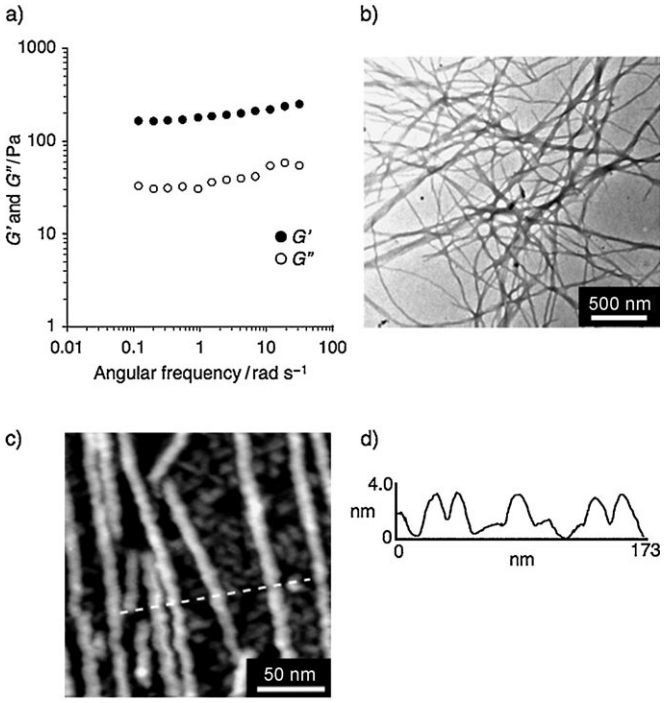

Figure 2. a) Oscillatory rheology frequency sweeps (0.15 wt%, distilled water); G': ●, G'': ○. b) TEM image of hydrogel **1** (0.10 wt%, distilled water, no staining), c) AFM image of the supramolecular fibers of **1** (see the Experimental Section for details), and d) the cross-section profile along the dotted line in c).

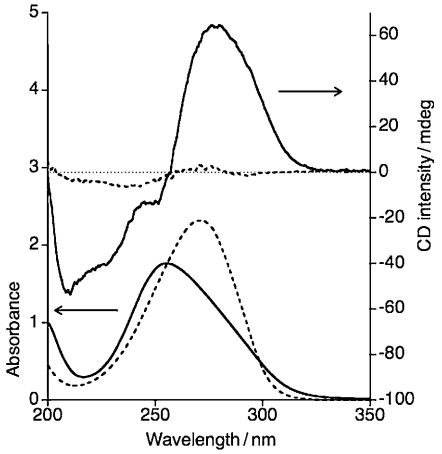

Figure 3. Absorption and CD spectra of **1** ([**1**] = 0.70 mM, 0.05 wt%) in the hydrogel state (——) and solution state (-----; 50% aqueous MeOH) in a 1 mm cell at ambient temperature.

cate that hydrogelator **1** self-assembles into a bilayer-type nanofiber and the subsequent bundling and entangling results in the hydrogel formation (Figure 1b), similar to hydrogelators **2** reported previously by us.[9,10] Interestingly, the unique fibrous structure of **1** could be visualized by atomic force microscopy (AFM). Figure 2c shows a typical AFM image of supramolecular fiber **1**. Careful analysis of the AFM micrograph allowed the average height of the nanofibers, 3 to 4 nm, to be determined. This height is slightly smaller than twice the molecular length of **1** and is comparable to the diameter of the interdigitated bilayer unit that was formed by the fibrous structure of **2** ($\approx$4 nm).[9c] It is also worth noting that the AFM micrograph clearly reveals a number of periodic oblique stripes that probably originate from a helical structure of the nanofiber.

Absorption and circular dichroism (CD) spectral measurements gave further insights into the molecular arrangement of **1** in the self-assembled fibers. The absorption and CD spectra of monomeric **1** in 50% aqueous MeOH were compared with those of hydrogel **1**. As shown in Figure 3, hydrogel **1** exhibited strong negative and positive CD signals in the region of λ = 200–325 nm, which can be assigned to a π–π^* transition of muconic amide, whereas monomeric **1** showed negligible CD signals.[11] This split Cotton effect resulting from the exciton coupling suggests that two muconic amide units are asymmetrically tilted in the hydrogel. The absorption spectrum for hydrogel **1** revealed a hypsochromic blueshift relative to the monomeric **1**, which indicates that the muconic amide units are closely interacting in a parallel manner in the gel matrix. From these results, we conclude that the muconic amide moieties of **1** are stacked with each other in a helical (preferably right-handed) fashion within the self-assembled nanofibers.

Confocal laser scanning microscopy (CLSM) observations of supramolecular hydrogel 1 to evaluate the mesh size: With the well-defined artificial glyco-lipid mimic hydrogelator **1** in hand, we explored the biological applications of this supramolecular hydrogel, in particular the encapsulation of live cells by the hydrogel matrix. To encapsulate live cells homogeneously in the networks of supramolecular hydrogels, it is important to control both the mesh size of the hydrogel and the homogeneous 3D distribution of the supramolecular fiber networks. Prior to cell culture experiments, we therefore evaluated the porosity of the hydrogel and the 3D dispersibility of the supramolecular fibers in **1** by using CLSM (see the Experimental Section for details).

To estimate the mesh size of hydrogel **1**, we evaluated the Brownian motion of submicron-sized polymer beads embedded in the hydrogel matrix by using CLSM according to our previously reported method.[9d,10a,12] The restricted Brownian motion of the beads can be ascribed to the fact that the mesh size in the hydrogel is comparable to the size of the beads. When we added 0.5 or 1.0 μm beads to hydrogel **1** (0.10 wt%, ion-exchanged water), the Brownian motion of the beads was almost perfectly restricted (Figure 4b for 0.5 μm beads). On the other hand, 0.1 μm beads showed moderate Brownian motion in hydrogel **1** (Figure 4a).[13] This result indicates that hydrogel **1** forms a nanomesh in which the lower size limit of the void has been evaluated to be smaller than 500 nm at 0.1 wt% of hydrogel, and the nanomesh is strong enough to be a physical obstacle to trap the beads. The size and toughness of the nanomesh constructed from hydrogel **1** is expected to be sufficient for the encapsulation of live cells.

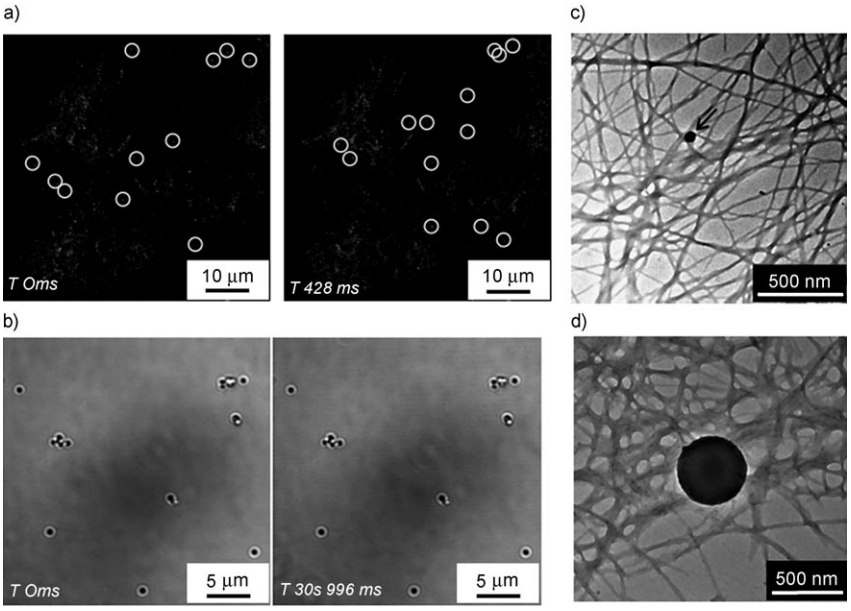

Figure 4. CLSM images of hydrogel **1** (0.10 wt %) stained with octadecyl rhodamine B chloride at ambient temperature (see the Experimental Section for details) in the presence of a) 0.1 μm plain beads (left = 0 and right = 0.4 s; fluorescence mode) and b) 0.5 μm plain beads (left = 0 and right = 30 s; DIC mode). TEM images of hydrogel **1** (0.10 wt %, no staining) in the presence of c) 0.1 and d) 0.5 μm plain beads. See the Supporting Information for the color version of Figure 4a.

Figure 4c and d show typical TEM images of hydrogel **1** with 0.1 and 0.5 μm beads, respectively. It is clear that the average widths of the nanofibers were almost the same as that observed in the absence of beads (Figure 2b), and the network structure of the supramolecular fibers was not destroyed. These results suggest that there would not be strong perturbation of the network of the supramolecular fibers from these nanobeads. In addition, the TEM images (Figures 2b and 4c,d) revealed that the apparent mesh size of hydrogel **1** is in the range of several hundreds of nm, which is consistent with the evaluation of the Brownian motion of the nanobeads. In fact, we could even find 0.1 μm beads entrapped within the nanomesh of the hydrogels, as shown in Figure 4c,d. More interestingly and unexpectedly, during the course of these careful experiments, we noticed that the 3D dispersibility of supramolecular fibers **1** was greatly improved in the presence of the beads (vide infra).

3D homogeneous distribution of supramolecular fibers of 1 induced by polymer nanobeads: We subsequently investigated the effects of the beads on the 3D homogeneous distribution of the supramolecular fibers in detail. CLSM *z*-stack images were obtained to evaluate the 3D dispersibility of fluorescently stained fibers of **1** in the gel state. Figure 5a shows typical low-magnified *z*-stack CLSM images of the hydrogel with varied height (*z* axis) in the presence or absence of 0.1 μm plain beads in microwells (diameter ≈7 mm), and careful analyses of the dependence of the fluorescence intensity on the *z* axis are shown in Figure 5b. The fiber content, as indexed by the fluorescence intensity, gradually decreased from the bottom of the well to the top in the absence of nanobeads, whereas the fluorescence intensity was almost constant from the bottom to the top in the presence of nanobeads. To our surprise, the 3D dispersibility of supramolecular fibers was significantly improved in the presence of the beads.

Next, the influence of the size and surface modification of the beads on the 3D dispersion of supramolecular fibers **1** was examined in detail, that is, we employed 0.05 to 1.0 μm polystyrene beads that had carboxyl groups or primary amine groups at their surfaces in addition to plain beads that had a small number of sulfate ester groups originating from the polymerization initiator. Figure 5c shows the normalized difference between the maximum and the minimum fluorescence intensities $((I_{max}-I_{min})/I_{max})$ depending on the size and type of bead used. This parameter indicates the degree of 3D dispersibility of the fibers, that is, the small value can be ascribed to homogeneously distributed fibers along the *z* axis (i.e., the depth profile) in the hydrogel. We found that the optimal bead sizes for the 3D dispersal of supramolecular fibers **1** are 0.1 and 0.5 μm. These beads were the most effective for homogeneous dispersion of the fibers, whereas 1.0 and 0.05 μm beads were less effective. 1.0 μm beads are probably too heavy to disperse homogeneously by themselves and so result in sedimentation, whereas 0.05 μm beads were too small to give a considerable interaction with the fiber networks. In addition, the concentration of the beads is another important factor and 1.1×10^{8} particles mL^{-1} was evaluated to be the optimal concentration for 0.1 μm and 0.5 μm beads. On the other hand, the surface chemistry of the beads (plain, anionic, or cationic; 0.1–1.0 μm diameter) did not significantly influence the 3D fiber distribution.

The mechanism of the 3D homogeneous distribution of the supramolecular fibers as facilitated by nanobeads still remains to be elucidated. We presume that appropriate sizes of beads would act as a noncovalent or dynamic cross-linker to facilitate the formation of the network of supramolecular fibers around the beads, although more effort is required to clearly understand the mechanism. Moreover, the rather homogeneous 3D hybrid matrix composed of supramolecular fibers **1** and nanobeads is anticipated to be potentially promising for encapsulating live cells in 3D.

The 3D encapsulation of live Jurkat cells: For the cell culture study, we initially confirmed that **1** could form a stable

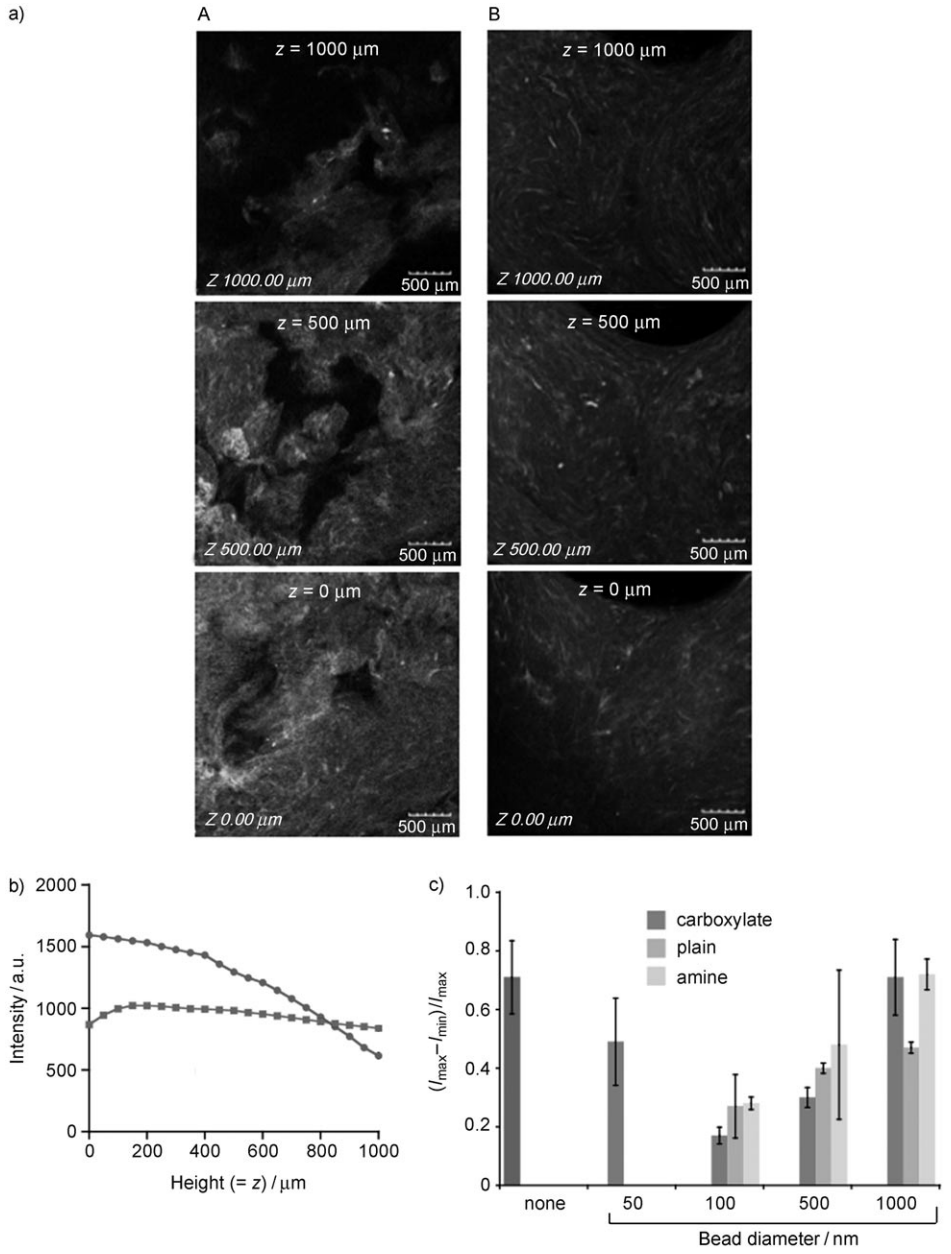

Figure 5. a) CLSM images of hydrogel **1** (0.10 wt %) stained with HANBD (HANBD = 7-*N*-methyl-*N*-[2-(2-hydroxyacetyl)ethoxy]amino-4-nitrobenzo-2-oxa-1,3-diazole)[9d] at ambient temperature (see the Experimental Section for details) in the absence (A) and presence (B) of 0.1 μm plain beads. b) Fluorescence intensity (integration of pixel intensity of images at each *z*-axis height) plots versus the *z*-axis height of the gels in A) (●) and B) (■). c) Fiber dispersion efficiency for each type of bead, which was evaluated from the normalized difference between maximum and minimum fluorescence intensities ($(I_{max}-I_{min})/I_{max}$). The mean and standard deviations of the values were estimated on the basis of at least three individual readings. See the Supporting Information for the color version of Figure 5.

hydrogel in cell culture media, such as RPMI 1641 and DMEM (RPMI = Roswell Park Memorial Institute medium, DMEM = Dulbecco's modified eagle medium). A human T-cell lymphoblast-like cell line (Jurkat) and a self-assembled artificial scaffold comprised of a supramolecular fibers **1**/nanobead hybrid were employed for the 3D cell encapsulation study. Figure 6a shows 3D CLSM images of Jurkat cells in RPMI with or without **1**/nanobeads after incubating for one day. Cell sedimentation was confirmed in RPMI in the absence of **1** (Figure 6a, A). In sharp contrast, the cells were partly three-dimensionally dispersed in the presence of the hydrogel (Figure 6a, B), and the 3D cell dispersion was further facilitated by the addition of 0.1 μm plain beads (Figure 6a, C). This result is ascribed to the fact that the nanobeads can induce the homogeneous dispersion of the supramolecular fiber networks and nanomesh in the hydrogel, which gives rise to effective 3D cell encapsulation in the supramolecular hybrid matrix. Figure 6b shows a typical magnified CLSM image of cells encapsulated in the supramolecular hybrid matrix, and reveals that the cells (yellow particles) are supported by the stiff network (red fibrils) of supramolecular fibers **1**, as depicted in Figure 6c.

A WST-8 assay (WST-8 = 2-(2-methoxy-4-nitrophenyl)-3-(4-nitrophenyl)-5-(2,4-disulfophenyl)-2H tetrazolium monosodium salt, see the Experimental Section) was conducted to check the cell proliferation under the three different conditions, including the supramolecular matrix comprised of hydrogel **1** and 0.1 μm plain beads. As shown in Figure 6d, the cells encapsulated in hydrogel **1** in the presence of beads can grow constantly for at least 6 d, which is longer than those in RPMI alone (i.e., without **1** or beads) or those in RPMI/**1** without beads. This result indicates that the hybrid matrix, similarly to the RPMI/supramolecular fibers **1** matrix, does not have considerable cytotoxicity.

Conclusion

We have demonstrated herein that the 3D homogeneous distribution of supramolecular nanofibers in hydrogel was

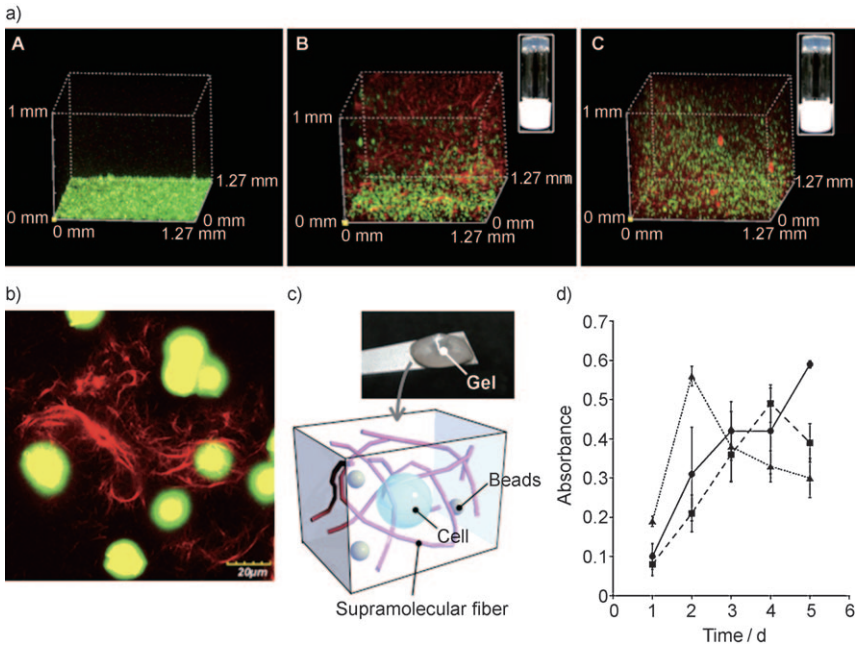

Figure 6. a) 3D CLSM images of Jurkat cells in RPMI 1641 only (A) and in RPMI 1641 and **1** (0.10 wt%) in the absence of (B) and presence of 0.1 μm plain beads (C); the insets show photographs of the cell culture gel **1**. The cells and supramolecular fibers were prelabeled with calcein AM and octadecyl rhodamine B chloride, respectively (see the Experimental Section for details). b) Magnified CLSM *z*-slice image of a) picture C, c) photograph of Jurkat cells encapsulated in RPMI 1641 and **1** (0.10 wt%) in the presence of 0.1 μm plain beads and the corresponding schematic representation (not drawn to scale), and d) quantification of cell survival A) in RPMI 1641 (•••••▲•••••), B) in RPMI 1641 and **1** (0.10 wt%) in the absence of 0.1 μm plain beads (-----■-----), and (C) in the presence of 0.1 μm plain beads (——●——), determined by using a WST-8 assay.

greatly facilitated by the addition of 100–500 nm polymer beads. Thanks to this unexpected effect, the 3D encapsulation and distribution of live cells in a supramolecular hydrogel comprised of artificial glyco-lipid **1** can be accomplished under physiological conditions. This kind of hybrid matrix composed of a supramolecular gel and nanobeads has rarely been explored.[14] We believe that such supramolecular hybrid matrices can be utilized as a unique scaffold for biomaterials.[15,16] The orthogonal modification of nanofibers and nanobeads and their cooperative behavior may lead to designable biomaterials, for instance, nanobeads with carboxylate and amine groups on their surfaces could be further functionalized through the introduction of a variety of bioactive molecules, such as RGD (Arg-Gly-Asp) peptide and growth factors, at controlled density and at the desired place. We are currently investigating in this direction.

Experimental Section

Materials and instruments: Unless stated otherwise, all commercial reagents were used as received. HANBD was synthesized according to our previously reported method.[9] The polymer microspheres (0.05, 0.1, 0.5, 1.0 μm) used in this study, termed as plain beads (polystyrene microspheres, slight anionic charge from sulfate ester groups), carboxylate beads (polystyrene microspheres that have surface carboxyl groups), and amino beads (polystyrene microspheres that have surface primary amine groups) were purchased from Polyscience (Warrington, PA, USA) as about 2.5% (w/v) solid aqueous suspensions and were used as received. Thin-layer chromatography (TLC) was performed on silica gel 60 F_{254} (Merck). Column chromatography was performed on silica gel 60 N (Kanto, 40–50 μm). ^{1}H NMR spectra were obtained by using a Varian Mercury 400 spectrometer with tetramethylsilane (TMS) or residual nondeuterated solvents as the internal references. FAB and MALDI-TOF mass spectra were recorded by using Shimadzu QP5050A (with NBA as a matrix) and PerSeptive Biosystems Voyager-DE RP instruments (with dithranol as a matrix), respectively. The absorption and CD spectra were measured by using a Shimadzu UV2550 spectrometer and a Jasco J-720WI spectropolarimeter, respectively. Rheological measurement was carried out by using a Reologica DynAlyser DAR-100 with a parallel plate (diameter 4.0 cm) at strain (0.10%) and gap (1.6 mm) at 24°C and the reproductivity of the data was confirmed by using at least two individual samples. Elemental analysis was carried out by the services at Kyoto University.

Syntheses: The typical procedure for the synthesis of hydrogelators with muconic amide in their spacer moiety is shown below. Compound **3**, derived from L-glutamic acid, and the sugar derivative (GlcNAc-NH_2) shown in Scheme 1 were synthesized according to a previously reported method.[9]

NHS derivative ***4***: $SOCl_2$ (400 μL, 2.5 equiv) and DMF (few drops) were added to a solution of muconic acid (320 mg, 2.3 mmol) in dry CH_2Cl_2

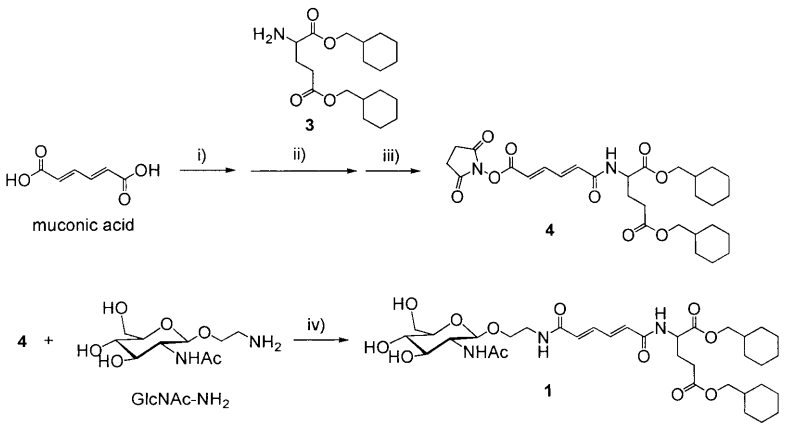

Scheme 1. Synthesis of hydrogelator **1**; i) $SOCl_2$, DMF, CH_2Cl_2; ii) DIPEA (*N*,*N*-diisopropylethylamine), CH_2Cl_2; iii) NHS (*N*-hydroxysuccinimide), BOP (benzotriazol-1-yloxytris(dimethylamino)phosphonium hexafluorophosphate), DIPEA, DMF (17% over three steps); iv) DIPEA, DMF (77%).

(10 mL) under a N_2 atmosphere. The reaction was heated at reflux for 10 h, after which the solution was concentrated under reduced pressure and dried in vacuo to give muconic chloride. The obtained muconic chloride was dissolved in dry CH_2Cl_2 (10 mL) and DIPEA (2.0 mL), then compound **3** (816 mg, 0.90 equiv) in dry CH_2Cl_2 (50 mL) was added dropwise to the solution over 30 min under a N_2 atmosphere. After stirring for an additional 20 min at RT, the solution was concentrated under reduced pressure. The residue was dissolved in chloroform (150 mL) and washed with 5% aqueous citric acid. The organic layer was dried over $MgSO_4$ and the solvent was removed under reduced pressure to afford an orange oil (1.07 g) that contained the target compound and a bola-type compound; the oil was used for next step without further purification. BOP (1.33 g, 1.3 equiv vs. muconic acid) and *N*-hydroxysuccinimide (346 mg, 1.3 equiv vs. muconic acid) were added to a solution of the obtained oil (1.07 g) and DIPEA (523 μL) in dry DMF (10 mL), and the resulting solution was stirred at 40 °C for 12 h. The solution was concentrated under reduced pressure and the obtained residue was dissolved in chloroform (150 mL) and washed with 5% aqueous citric acid. The organic layer was dried over $MgSO_4$ and the solvent was removed under reduced pressure, then the residue was purified by column chromatography (SiO_2, hexane/ethyl acetate 1:1) to afford compound **4** as a white solid (213 mg, 17% over three steps). ^{1}H NMR (400 MHz, $CDCl_3$, TMS, RT): $\delta = 7.54$ (dd, $J = 15.6$, 15.2 Hz, 1H; muconic-H), 7.30 (dd, $J = 14.8$, 15.3 Hz, 1H; muconic-H), 6.61 (d, $J = 4.4$ Hz, 1H; NH), 6.33 (d, $J = 15.6$ Hz, 1H; muconic-H), 6.32 (d, $J = 14.8$ Hz, 1H; muconic-H), 4.70 (t, $J = 4.4$ Hz, 1H; Glu-α-H), 3.97 (d, $J = 6.4$ Hz, 2H; OCH_2), 3.88 (d, $J = 6.4$ Hz, 2H; OCH_2), 2.86 (s, 4H; NHS-CH_2), 2.30–2.51 (m, 2H; Glu-γ-CH_2), 2.25, 2.06 (2×m, 2×1H; Glu-β-CH_2), 1.71–0.98 ppm (m, 22H; cyclohexyl-CH_2).

*GlcNAc derivative **1***: A solution of compound **4** (433 mg, 0.77 mmol), GlcNAc-NH_2 (245 mg, 0.93 mmol), and DIPEA (300 μL) in dry DMF (20 mL) was stirred at 40 °C for 12 h, then the solution was concentrated under reduced pressure. The resulting residue was washed with MeOH, diethyl ether, and cold water to afford compound **1** as a white powder (420 mg, 77%). ^{1}H NMR (400 MHz, $CDCl_3/CD_3OD$ 4:1, TMS, RT): $\delta =$ 7.21–7.25 (m, 2H; muconic-H), 6.30–6.35 (m, 2H; muconic-H), 4.61–4.64 (m, 1H; Glu-α-H), 4.41 (d, $J = 8.0$ Hz, 1H; GlcNAc-H[1]), 3.98 (m, 2H (overlapped with the peak of solvent); OCH_2), 3.89 (d, $J = 6.4$ Hz, 2H; OCH_2), 3.83–3.30 (m, 10H; GlcNAc-H and OCH_2CH_2NH), 2.39–2.43 (m, 2H; Glu-γ-CH_2), 2.23, 2.04 (2×m, 2×1H; Glu-β-CH_2), 2.00 (s, 3H; GlcNAc-CH_3CONH), 1.97–0.96 ppm (m, 22H; cyclohexyl-CH_2); HRMS (FAB, NBA, M^+): m/z calcd for $C_{35}H_{55}O_{12}N_3$: 709.3786; found: 709.3776; elemental analysis calcd (%) for $C_{35}H_{55}N_3O_{12}\cdot H_2O$: C 57.76, H 7.89, N 5.77; found: C 58.05, H 7.65, N 5.78.

Hydrogel preparation and confocal microscopy: Hydrogel **1** (0.10 wt%, 1.4 mM) was suspended in ion-exchanged water that contained either nitrobenzoxadiazole derivative (HANBD; final concentration = 20 μM, MeOH solution), which is an environmentally sensitive fluorophore that exhibits strong, blueshifted fluorescence in hydrophobic environments, such as the interior of self-assembled fibers constructed by hydrophobic interactions between alkyl moieties or octadecyl rhodamine B chloride (final concentration = 25 μM, MeOH solution, molecular probe, Invitrogen) for staining the hydrogel fiber. This suspension was heated by using a heat gun until a transparent homogeneous solution was obtained in both the absence and presence of beads (0.5 μL) in an aqueous dispersion at the appropriate ratio to **1** (200 μL). The hot solution (≈10 μL) was spotted on a glass-bottomed dish (Matsunami, noncoated, 0.15–0.18 mm glass bottom), incubated to complete gelation in a sealed box with high humidity at RT for 30 min, and then the sample was observed by using CLSM. CLSM observation is a powerful, convenient tool for the direct visualization of wet materials. By using this method, we can obtain structural insight into hydrogels without drying the sample. An inverted confocal laser scanning microscope (Olympus FV1000-ASW) equipped with a ×100, NA = 1.40 oil objective or a ×4, NA = 0.16 air objective and either a $\lambda = 543$ and 633 nm HeNe or a $\lambda = 488$ nm Ar laser was employed to obtain the images.

TEM observations: A suspension of **1** (0.10 wt%, 1.4 mM) in ion-exchanged water was heated in a 2 mL vial by using a heat gun until a transparent homogeneous solution was obtained in both the absence and presence of beads. The solution was incubated at RT for 30 min to complete gelation. The gel was placed on a copper TEM grid covered by an elastic carbon support film (20–25 nm) with a filter paper underneath, and the excess solution was blotted with the filter paper immediately. The TEM grid was dried under reduced pressure for at least 6 h prior to TEM observation. TEM images were acquired by using a JEOL JEM-1025 instrument (accelerating voltage 100 kV) equipped with a CCD camera.

AFM observations: A suspension of **1** (0.10 wt%, 1.4 mM) in ion-exchanged water (1.0 mL) was heated in a 2 mL vial by using a heat gun until a transparent homogeneous solution was obtained. The warm solution was diluted five-fold and immediately spread on freshly cleaved mica. The AFM observations were performed by using a Shimadzu SPM-9600 microscope in air at ambient temperature with standard silicon cantilevers (AR5-NCHR, Nanosensors) in the tapping mode.

Cell culture and confocal microscopy: Jurkat cells were maintained in RPMI 1641 medium supplemented with 10% fetal bovine serum (FBS). All media contained 1 wt% penicillin/streptomycin mixture. The cell incubation was always carried out at 37 °C in fully humidified air that contained 5% CO_2. For confocal micrographs of cells encapsulated in the hydrogels, a suspension of **1** (0.10 wt%, 1.4 mM) in cell culture medium (RPMI 1641) supplemented with 10% FBS was heated to form a homogeneous solution in both the absence and presence of beads. The resulting hot solution (50 μL) was immediately transferred to each well of a 96-well glass-bottomed culture plate (Iwaki). The solution of octadecyl rhodamine B chloride (final concentration = 25 μM) was subsequently added to each well to stain the hydrogel fiber, and the plate was then incubated for 3 h at 37 °C and 5% CO_2. RPMI 1641 medium (50 μL) was carefully added to the top of the gel, then the plate was placed in an incubator at 37 °C and 5% CO_2 and incubated for 24 h. Then, a suspension of Jurkat cells (50 μL, 3.0×10^6 mL^{-1}; pre-labeled with calcein AM according to the standard procedure supplied by the manufacture (DOJIN)) was transferred to each well. After 24 h, all wells were imaged by using a CLSM microscope (Olympus FV1000-ASW).

Cytotoxicity in hydrogel as determined by a WST-8 assay: The cell number was evaluated by using Cell-Counting Kit-8 (CCK-8, Dojindo, Japan), known as a WST-8 assay. The WST-8 assay uses a tetrazolium salt that produces a water-soluble formazan dye upon dehydrogenase-mediated reduction in the living cells. The hot solution of **1** (0.10 wt%, 50 μL of RPMI 1641 medium supplemented with 10% FBS) with or without beads was immediately transferred to a 96-well culture plate (Iwaki). RPMI 1641 medium (50 μL) was carefully added to the top of the gel and the plate was placed into an incubator at 37 °C and 5% CO_2 for 24 h. Then, a suspension of Jurkat cells (50 μL, 1.7×10^6 mL^{-1}) was transferred to each well. After each incubation period, the CCK-8 working solution (15 μL) was added to each well, and the cell suspensions were incubated for 3 h at 37 °C and 5% CO_2, then diluted four-fold just before measurements were taken. The plate was read by using a Wallac ARVO SX microplate reader (Perkin–Elmer) with a wavelength of 450 nm. After measurement, 50 μL of the medium on the top of the wells was exchanged. Each sample was tested in at least three wells, and the mean and standard deviation of the values were estimated.

Acknowledgements

This work is partially supported by JST (PRESTO, Synthesis and Control). S.M. thanks JSPS for the Research Fellowship for Young Scientists for financial support. We thank Dr. K. Kuwata (Kyoto university) for HRMS measurements, the members of Y. Aoyama laboratory (Kyoto university) for the use of and kind support with the plate reader, Dr. A. Narita (Y. Chujo laboratory, Kyoto university) for the TEM observations, and Prof. T. Takigawa (Kyoto university) for the rheometer observations.

[1] For reviews on supramolecular hydrogels, see: a) L. A. Estroff, A. D. Hamilton, *Chem. Rev.* **2004**, *104*, 1201–1217; b) M. de Loos,

B. L. Feringa, J. H. van Esch, *Eur. J. Org. Chem.* **2005**, 3615–3631; c) *Molecular Gels: Materials with Self-Assembled Fibrillar Networks*, (Eds.: R. G. Weiss, P. Terech), Springer, Dordrecht, The Netherlands, **2006**, Chapters 17 and 18; d) Z. Yang, B. Xu, *J. Mater. Chem.* **2007**, *17*, 2385–2393.

[2] For selected recent examples on supramolecular hydrogels, see: a) N. Sreenivasachaary, J.-M. Lehn, *Chem. Asian J.* **2008**, *3*, 134–139; b) K. M. Anderson, G. M. Day, M. J. Paterson, P. Byrne, N. Clarke, J. W. Steed, *Angew. Chem.* **2008**, *120*, 1074–1078; *Angew. Chem. Int. Ed.* **2008**, *47*, 1058–1062; c) M. Suzuki, T. Sato, H. Shirai, K. Hanabusa, *New J. Chem.* **2007**, *31*, 69–74; d) W. Deng, H. Yamaguchi, Y. Takashima, A. Harada, *Angew. Chem.* **2007**, *119*, 5236–5239; *Angew. Chem. Int. Ed.* **2007**, *46*, 5144–5147; e) Z. M. Yang, C. L. Liang, M. L. Ma, A. S. Abbah, W. W. Lu, B. Xu, *Chem. Commun.* **2007**, 843–845; f) I. Hwang, W. S. Jeon, H.-J. Kim, D. Kim, H. Kim, N. Selvapalam, N. Fujita, S. Shinkai, K. Kim, *Angew. Chem.* **2006**, *119*, 214–217; *Angew. Chem. Int. Ed.* **2006**, *46*, 210–213; g) D. Das, A. Dasgupta, S. Roy, R. N. Mitra, S. Debnath, P. K. Das, *Chem. Eur. J.* **2006**, *12*, 5068–5074.

[3] a) S. Zhang, T. C. Holmes, C. M. DiPersio, R. O. Hynes, X. Su, A. Rich, *Biomaterials* **1995**, *16*, 1385–1393; b) T. C. Holmes, S. de Lacalle, X. Su, G. Liu, A. Rich, S. Zhang, *Proc. Natl. Acad. Sci. USA* **2000**, *97*, 6728–6733; c) F. Gelain, A. Horii, S. Zhang, *Macromol. Biosci.* **2007**, *7*, 544–551, and references therein.

[4] G. A. Silva, C. Czeisler, K. L. Niece, E. Beniach, D. A. Harrington, J. A. Kessler, S. I. Stupp, *Science* **2004**, *303*, 1352–1355.

[5] L. Haines-Butterick, K. Rajogopal, M. Branco, D. Salick, R. Rughani, M. Pilarz, M. S. Lamm, D. J. Pochan, J. P. Schneider, *Proc. Natl. Acad. Sci. USA* **2007**, *104*, 7791–7796.

[6] a) K. Rajangam, H. A. Behanna, M. J. Hui, X. Q. Han, J. F. Hulvat, J. W. Lomasney, S. I. Stupp, *Nano Lett.* **2006**, *6*, 2086–2090; b) V. Jayawarna, M. Ali, T. A. Jowitt, A. F. Miller, A. Saiani, J. E. Gough, R. Ulijn, *Adv. Mater.* **2006**, *18*, 611–614;

[7] a) B. Geiger, A. Bershadsky, R. Pankov, K. M. Yamada, *Nat. Rev. Mol. Cell Biol.* **2001**, *2*, 793–805; b) B. Alberts, A. Johnson, J. Lewis, M. Raff, K. Roberts, P. Walter, *Molecular Biology of the Cell*, 4th ed., Garland Science, New York, USA, **2002**, Chapter 19.

[8] a) I.-J. Chen, H.-L. Chen, M. Demetriou, *J. Biol. Chem.* **2007**, *282*, 35361–35372; b) *Essentials of Glycobiology*, (Eds.: A. Varki, R. D. Cummings, J. D. Esko, H. H. Freeze, G. W. Hart, J. Marth), Cold Spring Harbor Laboratory, New York, USA, **1999**.

[9] a) S. Kiyonaka, K. Sugiyasu, S. Shinkai, I. Hamachi, *J. Am. Chem. Soc.* **2002**, *124*, 10954–10955; b) S. Kiyonaka, S. Shinkai, I. Hamachi, *Chem. Eur. J.* **2003**, *9*, 976–983; c) S. Kiyonaka, K. Sada, I. Yoshimura, S. Shinkai, N. Kato, I. Hamachi, *Nat. Mater.* **2004**, *3*, 58–64; d) S. Yamaguchi, S. Matsumoto, K. Ishizuka, Y. Iko, K. V. Tabata, H. F. Arata, H. Fujita, H. Noji, I. Hamachi, *Chem. Eur. J.* **2008**, *14*, 1891–1896.

[10] a) S. Matsumoto, S. Yamaguchi, S. Ueno, H. Komatsu, M. Ikeda, K. Ishizuka, Y. Iko, K. V. Tabata, H. Aoki, S. Ito, H. Noji, I. Hamachi, *Chem. Eur. J.* **2008**, *14*, 3977–3986; b) S. Matsumoto, S. Yamaguchi, A. Wada, T. Matsui, M. Ikeda, I. Hamachi, *Chem. Commun.* **2008**, 1545–1547.

[11] We checked that the contribution from the linear dichroism (LD) signal was negligible under these conditions by rotating the cell around the light axis.

[12] a) A. P. Nowak, V. Breedveld, L. Pakstis, B. Ozbas, D. J. Pine, D. Pochan, T. J. Deming, *Nature* **2002**, *417*, 424–428; b) T. G. Mason, K. Ganesan, J. H. van Zanten, D. Wirtz, S. C. Kuo, *Phys. Rev. Lett.* **1997**, *79*, 3282–3285.

[13] We should note that it was not possible to determine whether all the 0.1 μm beads diffused in the gel freely or rather restrictedly.

[14] For examples of supramolecular organogel-nanoparticle composites, see: a) J. van Herrikhuyzen, S. J. George, M. R. J. Vos, N. A. J. M. Sommerdijk, A. Ajayaghosh, S. C. J. Meskers, A. P. H. J. Schenning, *Angew. Chem.* **2007**, *119*, 1857–1860; *Angew. Chem. Int. Ed.* **2007**, *46*, 1825–1828; b) S. Bhattacharya, A. Srivastava, A. Pal, *Angew. Chem.* **2006**, *118*, 3000–3003; *Angew. Chem. Int. Ed.* **2006**, *45*, 2934–2937; c) M. Kimura, S. Kobayashi, T. Kuroda, K. Hanabusa, H. Shirai, *Adv. Mater.* **2004**, *16*, 335–338; d) B. Simmons, S. Li, V. T. John, G. L. McPherson, C. Taylor, D. K. Schwartz, K. Maskos, *Nano Lett.* **2002**, *2*, 1037–1042.

[15] a) M. M. Stevens, J. H. George, *Science* **2005**, *310*, 1135–1138; b) L. G. Griffith, M. A. Swartz, *Nat. Rev. Mol. Cell Biol.* **2006**, *7*, 211–224.

[16] a) M. C. Cushing, K. S. Anseth, *Science* **2007**, *316*, 1133–1134; b) P. Y. W. Dankers, E. W. Meijer, *Bull. Chem. Soc. Jpn.* **2007**, *80*, 2047–2073; c) R. V. Ulijn, *J. Mater. Chem.* **2006**, *16*, 2217–2225; d) M. P. Lutolf, J. A. Hubbell, *Nat. Biotechnol.* **2005**, *23*, 47–55; e) S. Zhang, *Nat. Biotechnol.* **2004**, *22*, 151–152; f) Y. Luo, M. S. Shoichet, *Nat. Mater.* **2004**, *3*, 249–253.

Received: June 11, 2008
Published online: October 22, 2008

